JCI insight

Sex-dependent factors encoded in the immune compartment dictate relapsing or progressive phenotype in demyelinating disease

Tessa Dhaeze, … , Stephanie Zandee, Alexandre Prat

JCI Insight. 2019;4(6):e124885. https://doi.org/10.1172/jci.insight.124885.

Research Article Neuroscience

TCR^{1640} mice, which have a T cell receptor (TCR) directed against $MOG^{92–106}$, spontaneously develop experimental autoimmune encephalomyelitis. Female mice mostly develop a relapsing-remitting (RR) course and have a higher incidence of disease, while males most frequently suffer from progressive disease, reflecting the unresolved clinical sex discrepancies seen in multiple sclerosis. Herein, we performed adoptive transfers of male and female TCR^{1640} immune cells into WT animals to investigate if disease course is dependent on the sex of the donor immune cells or on the sex of the recipient animal. We found that transfer of female TCR^{1640} immune cells led to a RR disease while transfer of male TCR^{1640} immune cells led to a progressive course, independent of the sex of the recipient. In addition, regulatory and pathogenic T cell infiltration after transfer was also immune cell sex intrinsic. We performed genetic profiling of the donor immune cells and found significant differences between the transcriptomic profiles of male and female TCR^{1640} immune cells, interestingly, within genes related to immune regulation of T lymphocytes. These results suggest that differences in gene expression profiles related to regulation of T cell immunity seen in male and female neuroinflammatory disease drive relapsing versus progressive disease course.

JCI insight

RESEARCH ARTICLE

Sex-dependent factors encoded in the immune compartment dictate relapsing or progressive phenotype in demyelinating disease

Tessa Dhaeze,[1] Catherine Lachance,[1] Laurence Tremblay,[1] Camille Grasmuck,[1] Lyne Bourbonnière,[1] Sandra Larouche,[1] Olivia Saint-Laurent,[1] Marc-André Lécuyer,[1] Rose-Marie Rébillard,[1] Stephanie Zandee,[1] and Alexandre Prat[1,2]

[1]Neuroimmunology Unit, Department of Neuroscience, Faculty of Medicine, Université de Montréal, and Centre de recherche du CHUM (CRCHUM), Montréal, Québec, Canada. [2]Multiple Sclerosis Clinic, Division of Neurology, Centre hospitalier de l'Université de Montréal (CHUM), Montréal, Quebec, Canada.

TCR^{1640} mice, which have a T cell receptor (TCR) directed against MOG$^{92–106}$, spontaneously develop experimental autoimmune encephalomyelitis. Female mice mostly develop a relapsing-remitting (RR) course and have a higher incidence of disease, while males most frequently suffer from progressive disease, reflecting the unresolved clinical sex discrepancies seen in multiple sclerosis. Herein, we performed adoptive transfers of male and female TCR^{1640} immune cells into WT animals to investigate if disease course is dependent on the sex of the donor immune cells or on the sex of the recipient animal. We found that transfer of female TCR^{1640} immune cells led to a RR disease while transfer of male TCR^{1640} immune cells led to a progressive course, independent of the sex of the recipient. In addition, regulatory and pathogenic T cell infiltration after transfer was also immune cell sex intrinsic. We performed genetic profiling of the donor immune cells and found significant differences between the transcriptomic profiles of male and female TCR^{1640} immune cells, interestingly, within genes related to immune regulation of T lymphocytes. These results suggest that differences in gene expression profiles related to regulation of T cell immunity seen in male and female neuroinflammatory disease drive relapsing versus progressive disease course.

Introduction

Multiple sclerosis (MS) is considered an autoimmune disease of the CNS, as proinflammatory immune cells localize to the CNS parenchyma, the cerebrospinal fluid, and the meninges of MS patients, leading to oligodendrocyte death, myelin sheath destruction, and axonal damage. Clinically, MS is subdivided in different types of disease and disease phases based on recurrent and transient episodes of disability. At the time of diagnosis, the majority (roughly 85%) of patients will present with a relapsing-remitting form of the disease (RRMS) in which the occurrence of symptoms (relapses) is typically followed by periods of partial or complete recovery (remission). In about half of RRMS cases, the disease will evolve into a secondary progressive phase (SPMS), with steady progression of handicap over several years. In primary progressive MS (PPMS, 10%–15%), there is a steady worsening of neurological function without intermittent recovery. Intriguingly, a role for sex can be attributed to different disease phases, in that women mostly develop RRMS and are affected more (2–3:1) then men and that men seem to be overrepresented within the PPMS population (1). In addition to the higher risk for a woman to develop MS, men, in general, seem to develop more severe disease than women. Therefore, an involvement of sex in the disease pathophysiology likely contributes to both disease phenotype and severity, which could reveal clues for future treatment options. However, to date little is known about the underlying processes that dictate sex-specific differences in MS incidence and disease severity (2–4).

Transgenic TCR^{1640} mice express a T cell receptor (TCR) specific for rat/mouse MOG$^{92–106}$ and were first described by Wekerle's lab (5). This TCR was isolated from an encephalitogenic Th1 CD4$^+$ T cell clone on a SJL/j background and uses Vα8.3 and Vβ4 genes. Spontaneous experimental autoimmune encephalomyelitis–like (EAE-like) disease occurs in about 80% of the females and 60% of the males.

Conflict of interest: The authors have declared that no conflict of interest exists.

Submitted: September 20, 2018
Accepted: February 5, 2019
Published: March 21, 2019.

Reference information: *JCI Insight.* 2019;4(6):e124885. https://doi.org/10.1172/jci.insight.124885.

Females mostly develop spontaneous RR disease, while spontaneous progressive disease was more frequent in male TCR^{1640} mice. In addition, lesion development in this transgenic mouse model is not solely located in the spinal cord but also in the brain. This mouse model therefore provides a proxy to MS by exhibiting different disease courses (progression and remission), by radial development of lesions, and by exposing sex differences as seen in human MS patients.

In this manuscript, we aimed at revealing sex-dependent mechanisms that are able to influence disease type. Herein, we performed multiple adoptive transfers using immune cells isolated from the spleens and lymph nodes of female or male TCR^{1640} mice to investigate if disease type is driven by the sex of the donor or by the sex of the recipient. Subsequently, we studied whether sex-dependent factors influence immune cell phenotypes and infiltration into the CNS.

Results

Disease course after adoptive transfer with transgenic TCR^{1640} immune cells is dependent on the sex of the donor. TCR^{1640} mice, who have a transgenic TCR specific to MOG$^{92–106}$ and spontaneously develop EAE, were donated to our lab by the Hartmut Wekerle group (5). It was described that both incidence and type of disease differed between male and female TCR^{1640} mice, and we confirmed these results (Supplemental Figure 1A; supplemental material available online with this article; https://doi.org/10.1172/jci.insight.124885DS1). Histological analysis of the CNS revealed severe infiltration and demyelination during disease, as previously described (5) (Supplemental Figure 1B). We also confirmed that the majority of CNS-infiltrating cells were CD4$^+$ and both Th1 and Th17 lymphocytes were present (Supplemental Figure 1C) in both male and female animals.

In addition, we found that, apart from CD4$^+$ T lymphocyte infiltration, substantial changes can be detected at the level of the blood-brain barrier (BBB) during disease when comparing different disease phases: presymptomatic (day 35–40), acute disease (score ≥ 3), remission (recovery of score with Δ2), and primary progressive disease (stable disease score after progression ≥20 days). We observed a disruption of the vascular basal lamina accompanied by an infiltration of macrophages as well as perivascular and parenchymal deposition of fibrinogen during the presymptomatic phase of the disease and more so during acute attacks or during progressive disease (Supplemental Figures 2 and 3). The disrupted basal lamina was less obvious during remission, confirming radiological-based evidence of BBB restoration between clinical attacks (6). Interestingly, infiltration of macrophages into the parenchyma was most pronounced in primary progressive disease, despite a general upregulation of VCAM-1 across all disease phases (Supplemental Figures 2 and 3).

Given that this transgenic mouse model reflects human MS disease better than other EAE models, we sought out to investigate if the sex-related disease differences are immune intrinsic or dependent on the sex of the recipient. Overall, the adoptive transfers were performed as described in Figure 1A. Immune cells were isolated from secondary lymphoid organs (SLOs) of presymptomatic transgenic female and male TCR^{1640} mice, as well as their WT SJL/j littermates, and differentiated toward a Th1/Th17 phenotype. After differentiation, total immune cells were injected i.v. into female or male WT SJL/j littermates. Two days after injection, all mice were injected i.p. with pertussis toxin and scored daily over 60 days to analyze disease course. Disease course was quantified by giving a global clinical score based on both paralysis and ataxia.

Prior to adoptive transfer, the immune cells were characterized (Figure 1, B–D). The differentiated immune cells isolated from male and female TCR^{1640} mice and from WT animals had a significantly higher number of CD4$^+$ T lymphocytes compared with the small fraction of CD8$^+$ cells was present (Figure 1B). Given that CD4$^+$ T lymphocytes compose the majority of the cell population, the number of cells expressing the transgenic Vα8.3$^+$/Vβ4$^+$ TCR was analyzed and, as expected, was significantly higher in both female and male TCR^{1640} mice, compared with their WT littermates (Figure 1C). We then elected to analyze expression of IFN-γ and IL-17 (Th1/Th17 phenotype), GM-CSF production, and Foxp3 expression by CD4$^+$ T lymphocytes obtained from female and male TCR^{1640} mice to identify differences in their profiles that could explain disease phenotypes. Our data demonstrate that there was no difference in cytokine or regulatory profiles that could be either associated with or attributable to sex or disease phenotype (Figure 1D).

Next, to investigate if disease course is dictated by the sex of donor cells or by the sex of the recipient, female or male transgenic TCR^{1640} differentiated immune cells were injected into female

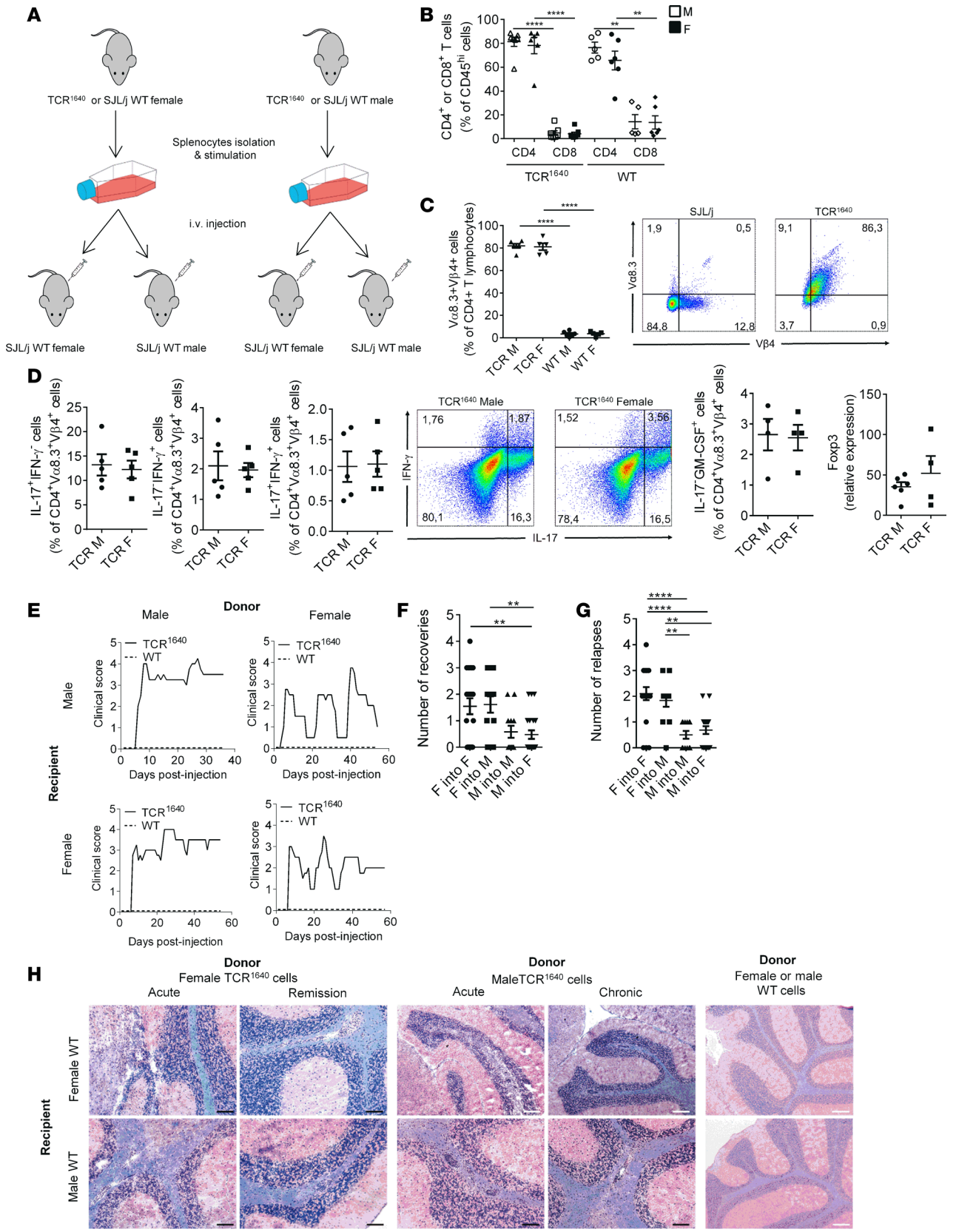
A
TCR1640 or SJL/j WT female
TCR1640 or SJL/j WT male
Splenocytes isolation & stimulation
i.v. injection
SJL/j WT female
SJL/j WT male
SJL/j WT female
SJL/j WT male
B
CD4+ or CD8+ T cells (% of CD45hi cells)
M
F
CD4
CD8
CD4
CD8
TCR1640
WT
C
Vα8.3+Vβ4+ cells (% of CD4+ T lymphocytes)
TCR M
TCR F
WT M
WT F
SJL/j
TCR1640
1,9
0,5
84,8
12,8
9,1
86,3
3,7
0,9
Vα8.3
Vβ4
D
IL-17+IFN-γ- cells (% of CD4+Vα8.3+Vβ4+ cells)
IL-17-IFN-γ+ cells (% of CD4+Vα8.3+Vβ4+ cells)
IL-17+IFN-γ+ cells (% of CD4+Vα8.3+Vβ4+ cells)
TCR M
TCR F
TCR1640 Male
TCR1640 Female
1,76
1,87
80,1
16,3
1,52
3,56
78,4
16,5
IFN-γ
IL-17
IL-17-GM-CSF+ cells (% of CD4+Vα8.3+Vβ4+ cells)
Foxp3 (relative expression)
E
Donor
Male
Female
Recipient
Male
Female
TCR1640
WT
Clinical score
Days post-injection
F
Number of recoveries
F into F
F into M
M into M
M into F
G
Number of relapses
F into F
F into M
M into M
M into F
H
Donor
Female TCR1640 cells
Acute
Remission
Donor
MaleTCR1640 cells
Acute
Chronic
Donor
Female or male WT cells
Recipient
Female WT
Male WT

Figure 1. Disease course after adoptive transfer with transgenic TCR^{1640} immune cells is dependent on the sex of the donor. (**A**) Overview of adoptive transfer where immune cells were isolated from spleens and lymph nodes of female and male TCR^{1640}-transgenic mice and WT SJL/j mice and differentiated toward a Th1/Th17 phenotype and were injected into WT SJL/j female and male recipients. (**B–D**) Analysis of immune cells isolated from female and male TCR^{1640}-transgenic and WT SJL/j mice and used for adoptive transfer. (**B**) Proportion of CD4$^+$ and CD8$^+$ T lymphocytes present in immune cells from TCR^{1640}-transgenic and WT SJL/j mice ($n \geq 5$ for each). (**C**) Average and representative dot plot of Vα8.3$^+$Vβ4$^+$ cells within CD4$^+$ T lymphocytes from TCR^{1640}-transgenic and WT SJL/j mice ($n \geq 5$ for each). (**D**) Representative FACS dot plot and average of Th1-, Th17-, and GM-CSF–producing cells and relative mRNA expression of Foxp3 (by qPCR) in female and male TCR^{1640}-transgenic mice ($n \geq 4$ for each). (**E**) Clinical disease courses of representative recipients after adoptive transfer with TCR^{1640} immune cells (—) or WT SJL/j immune cells (- - -) into WT SJL/j in different conditions (female into female, female into male, male into male and male into female). Graphs are representative of more than 3 independent experiments. (**F**) Number of recoveries to a clinical score of 0/1 counted in different adoptive transfer conditions. (**G**) Number of relapses (clinical score of $\Delta \geq 2$) counted in different adoptive transfer conditions. (**H**) Histological analysis using Luxol fast blue and counterstained by H&E of cerebellum of SJL/j female and male recipients after adoptive transfer. After injection of female TCR^{1640} immune cells, recipients were sacrificed at acute disease (first peak, score ≥3) and during remission (clinical score of $\Delta \geq 2$). After injection of male TCR^{1640} immune cells, recipients were sacrificed at acute disease (score ≥3) and during chronic disease (clinical score ≥3 for more than 20 days). Histological analysis of cerebellum of SJL/j injected mice was performed as a control. Scale bar: 100 μm (white); 250 μm (black). Data are representative of 3 or more independent experiments, with at least 3 mice per group. Data are represented as mean ± SEM, and an unpaired 1-sided *t* test or 1-way ANOVA was used. $^{**}P < 0.01$, $^{****}P < 0.0001$. $P < 0.05$ was considered significant.

or male WT SJL/j littermates (Figure 1, E–H). Progressive disease was defined by the presence and progression of neurological signs of disease, reaching clinical scores of at least 3, in the absence of significant recovery (Δ2 score). Relapsing-remitting (RR) disease was characterized by multiple relapses reflected by a Δ of clinical scores of at least 2, between the maximum score at relapse and minimum score at remission. As expected, female or male WT SJL/j differentiated immune cells injected into WT recipient animals did not induce clinical signs of neurological dysfunction (Figure 1E, dotted line for all graphs, and Figure 1H). However, injection of male TCR^{1640} immune cells into female or male WT littermates induced a progressive disease course without recovery (Figure 1E, representative graph, top). Interestingly, injection of female TCR^{1640} immune cells into female or male WT littermates induced a RR disease course (Figure 1E, representative graph, bottom). To quantify the disease course, the number of recoveries (defined by a recovery back to score 1) and the number of relapses (defined by a score of Δ2) were analyzed for each recipient. Injection of female TCR^{1640} immune cells into female or male WT SJL/j littermates induced a significantly higher amount of recoveries (Figure 1F, Table 1, and Supplemental Figure 4) and relapses (Figure 1G, Table 1, and Supplemental Figure 4) compared with injection of male TCR^{1640} immune cells. Interestingly, the sex of the recipient did not affect the type of disease (Figure 1, E–G, and Supplemental Figure 4). H&E staining of the CNS of recipient animals, combined with Luxol fast blue, revealed that, in all animals receiving transgenic immune cells, cell infiltrates were found mostly in the cerebellum (Figure 1H), in the surrounding meninges and in the ventricles (Supplemental Figure 5A), and that very few infiltrating cells were found in the spinal cord (Supplemental Figure 5B). The histological patterns observed in female and male recipients after receiving female transgenic immune cells showed demyelination associated with major infiltration at peak of the disease, but less so during remission (Figure 1H). Injection of male transgenic immune cells also led to demyelination, with substantial infiltration at peak and during the chronic phase. Consistent with the clinical observations, the animals receiving differentiated immune cells from WT animals did not have any cell infiltrates in their CNS (Figure 1H, right). In conclusion, adoptive transfer of female transgenic immune cells induces a RR disease, while injection of male transgenic immune cells leads to a primary progressive disease course, independent of the sex of the recipient. However, we did not detect major histological differences between recipients of either male or female TCR^{1640} immune cells, which could explain disease phenotype.

Regulatory and pathogenic T cell infiltration after adoptive transfer is driven by the sex of the transgenic donor cells and not by the recipient. To analyze pathological differences between female and male recipients after receiving either male or female TCR^{1640}-transgenic immune cells, immune cells infiltrating the CNS were recovered at different time points (acute phase, remission for female, and chronic phase for male). We found that the majority of CNS-infiltrating transgenic cells were CD4$^+$ T lymphocytes compared with CD8$^+$ T lymphocytes, in both mice receiving female TCR^{1640}-transgenic immune cells and mice receiving male TCR^{1640}-transgenic immune cells (Figure 2A and Figure 2B, respectively). After injection of female transgenic cells (Figure 2A), the absolute number of Vα8.3$^+$/Vβ4$^+$ CD4$^+$ lymphocytes in female and male recipients did not differ during the acute phase. However, there was a significant reduction of Vα8.3$^+$/Vβ4$^+$ CD4$^+$ lymphocytes in female recipients of female transgenic TCR^{1640} immune cells, compared with male recipients (Figure 2A).

Table 1. Overview of adoptive transfers

Donor	Recipient	*n*	*N*	Incidence (%)	RRMS (%)	PPMS (%)	Undetermined (%)
TCR F	WT F	20	3	100	70	30	0
TCR F	WT M	13	2	100	70	23	7
TCR M	WT M	12	2	100	16.7	66.6	16.7
TCR M	WT F	21	3	100	23	67	9.5
WT F	WT F	3	2	0	0	0	0
WT F	WT M	5	2	0	0	0	0
WT M	WT M	3	2	0	0	0	0
WT M	WT M	4	2	0	0	0	0

Overview of the number of mice used (*n*) and the number of independent experiments performed (*N*) per adoptive transfer. Incidence and type of disease were determined. RRMS, relapsing-remitting MS; PPMS, primary progressive MS; F, female; M, male.

This observation supported the clinical phenotype that was observed when immune cells of the same sex were injected, that is a stronger phenotype (RR disease or progressive disease) was seen, although this was not significant (data not shown). After injection of male transgenic cells (Figure 2B), no significant difference could be detected in the absolute number of transgenic cells between female or male recipients at any disease phase. Interestingly, no significant decrease in the percentage of infiltrating Vα8.3$^+$/Vβ4$^+$ CD4$^+$ or CD8$^+$ T lymphocytes was seen after injection of female transgenic immune cells (Figure 2C). A significant decrease in the percentage of infiltrating Vα8.3$^+$/Vβ4$^+$ cells at chronic disease after injection of male transgenic immune cells was only seen for CD4$^+$ T lymphocytes (Figure 2D). Since CD4$^+$ lymphocytes are most abundant in the CNS after adoptive transfer, we used immunofluorescent staining to localize them. CD4$^+$ immune cell infiltrates could be found in the cerebellum, the meninges, and the ventricles of animals receiving either female or male TCR^{1640}-transgenic immune cells (Figure 2E and Figure 2F, respectively).

Given that the major immune cell infiltrates were located in the cerebellar white matter, we focused on this brain region to compare female and male recipients after injection of transgenic immune cells for our analysis of Tregs. CD4$^+$FOXP3$^+$ infiltrating cells were found throughout the brains of recipient males and females at peak of disease (acute) after adoptive transfer. Interestingly however, these Tregs were found more clustered and more frequent within the infiltrates at remission after adoptive transfer of female TCR^{1640}-transgenic immune cells, independent of the sex of the recipient (Figure 2, G and I). CD4$^+$FOXP3$^+$ cells were observed in the brains of chronic animals that received male TCR^{1640}-transgenic immune cells, but no clustering was observed (Figure 2, H and J).

Both Th1 (IL-17$^-$IFN-γ$^+$) and Th17 (IL-17$^+$IFN-γ$^-$) lymphocytes are significantly increased in mice developing spontaneous TCR^{1640} EAE (5). Therefore, we hypothesized that variable proportions of these cells could explain distinct disease phenotype (remitting vs. progressive). When inducing disease using male TCR^{1640} immune cells, the percentage of Th17 lymphocytes decreased between acute and chronic phases, while the percentage of Th1 lymphocytes increased, in both male and female recipients (Figure 2K). When inducing disease using female TCR^{1640} immune cells, a similar trend was observed when comparing first peak with remission, although it was not as profound (Figure 2L).

Collectively, these data indicate that injection of male TCR^{1640} immune cells into either male or female recipients induces a IFN-γ–driven chronic disease, while injection of female TCR^{1640} immune cells into either male or female recipients induces an increased clustering of Foxp3$^+$ cells during remission, highlighting again that disease course is dependent on sex of the donor cells and independent on the sex of the recipient.

BBB disruption is similar between female and male recipients after adoptive transfer of either male or female TCR^{1640}-transgenic cells. To further compare if the underlying pathogenesis differs between female and male recipients after adoptive transfer of either female or male TCR^{1640}-transgenic immune cells, changes in BBB kinetics were analyzed. Visualization of leakage into the parenchyma through the BBB was done by staining for the blood coagulation protein fibrinogen, and activation of BBB endothelium was analyzed by upregulation of vascular cell adhesion protein 1 (VCAM-1). We found that the sites of upregulation of VCAM-1 on BBB endothelium and leakage of fibrinogen into the parenchyma colocalized with the presence of CD4$^+$ infiltrates, more specifically in the cerebellum, the surrounding meninges, and the ventricles after injection of both female and male TCR^{1640}-transgenic immune cells (Figure 3A).

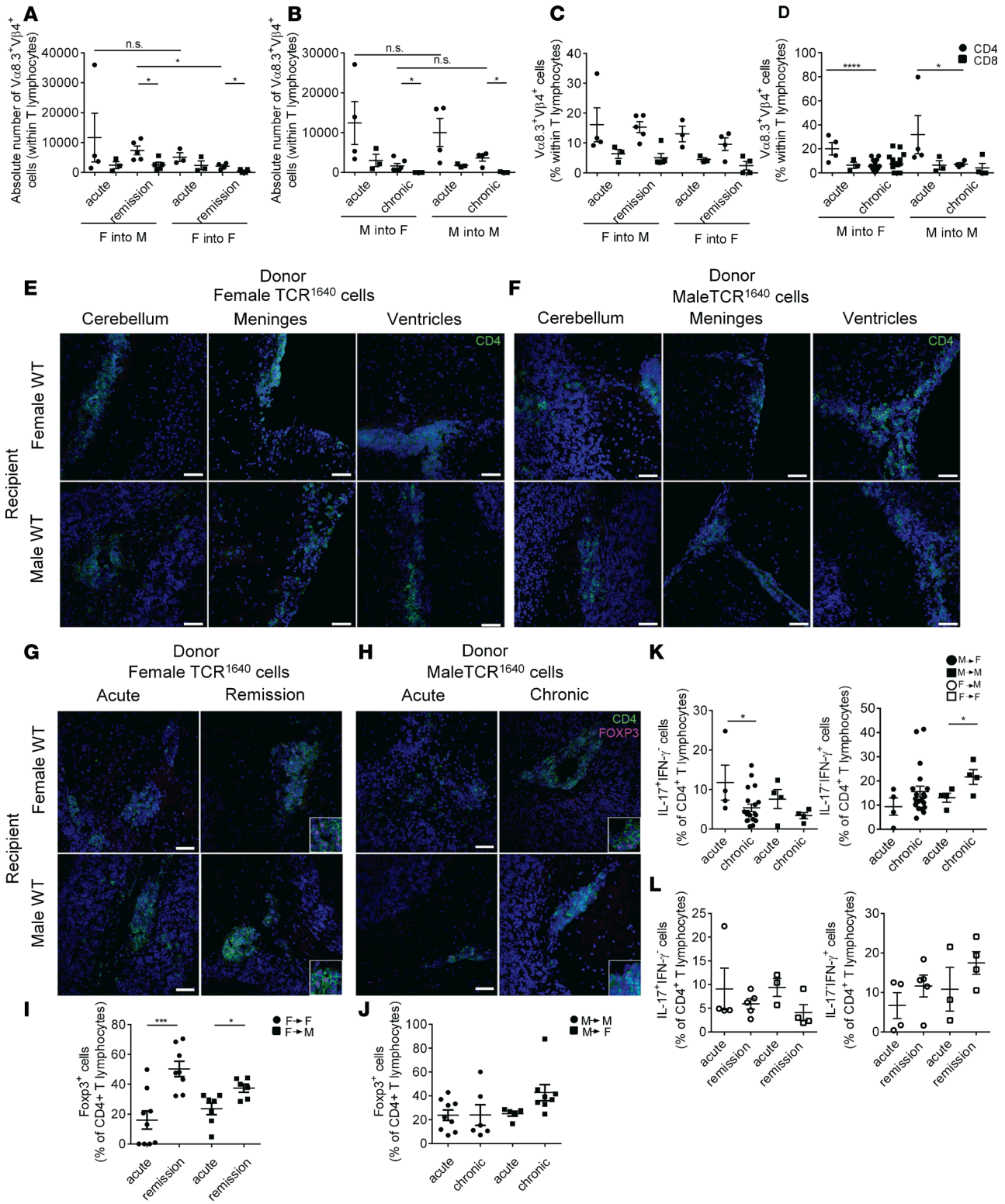

Figure 2. Regulatory and pathogenic T cell infiltration after adoptive transfer is driven by the sex of the transgenic donor cells and not by the recipient. Immune cell infiltration was analyzed after adoptive transfer in recipient animals sacrificed at first peak of disease (acute, clinical score ≥3) for all transfers, at remission (clinical score of Δ ≥2) for injection of female transgenic cells, and during chronic disease for injection of male transgenic cells (stable clinical score ≥3 for more than 20 days). (**A** and **B**) Absolute number of Vα8.3$^+$Vβ4$^+$ cells within CD4$^+$ T lymphocytes or CD8$^+$ T lymphocytes within the CNS of male and female SJL/j recipients at different disease phases after adoptive transfer of (**A**) female TCR^{1640} immune cells or (**B**) male TCR^{1640} immune cells. (**C** and **D**) Percentage of Vα8.3$^+$Vβ4$^+$ cells within CD4$^+$ T lymphocytes or CD8$^+$ T lymphocytes within the CNS of male and female SJL/j recipients at different disease phases after adoptive transfer of (**A**) female TCR^{1640} immune cells or (**B**) male TCR^{1640} immune cells. (**E** and **F**) Representative confocal images of CD4$^+$ T lymphocyte infiltration into cerebellum, meninges, and ventricles within the CNS of male and female SJL/j recipients at different disease phases after adoptive transfer of (**E**) female TCR^{1640} immune cells or (**F**) male TCR^{1640}

immune cells. (**G** and **H**) Representative confocal images of CD4+ T lymphocyte infiltration and infiltration of Foxp3+ cells into cerebellum of male and female SJL/j recipients at different disease phases after adoptive transfer of (**G**) female TCR^{1640} immune cells or (**H**) male TCR^{1640} immune cells. (**I** and **J**) Number of CD4+ and Foxp3+ cells from confocal images of cerebellum of male and female SJL/j recipients at different disease phases after adoptive transfer were counted and used to calculate the percentage of infiltrating Foxp3+ cells (at least 3 images were used per recipient). (**K** and **L**) Percentage of Th1 and Th17 lymphocytes in CNS of male and female SJL/j recipients at different disease phases after adoptive transfer of (**K**) male TCR^{1640} immune cells or (**L**) female TCR^{1640} immune cells. Data are representative of 3 or more independent experiments, with at least 3 mice per group Data are represented as mean ± SEM, and an unpaired 1-sided *t* test was used. *$P < 0.05$, *** $P < 0.001$, **** $P < 0.0001$. Scale bar: 100 μm. $P < 0.05$ was considered significant

Focusing again on the cerebellar white matter to compare recipients, we found that injection of female TCR^{1640}-transgenic immune cells induced upregulation of VCAM-1 and extravasation of fibrinogen in both female and male recipients (Figure 3B, left). During remission, we still observed leakage and deposition of fibrinogen into the parenchyma, although more dispersed, and upregulation of VCAM-1 was also still present in both recipients (Figure 3B, right). Injection of male TCR^{1640}-transgenic immune cells induced a similar pattern of BBB changes, as described for female injected recipients during the acute phase, and showed that BBB activation and fibrinogen extravasation and deposits were still present at chronic disease (Figure 3C). Quantification of VCAM-1 intensity and fibrinogen accumulation in recipients of female transgenic immune cells and recipients of male transgenic immune cells did not reveal significant differences (Figure 3D).

In conclusion, we observed major changes in BBB kinetics shown by VCAM-1 upregulation and fibrinogen extravasation in all phases of the disease course after adoptive transfer of both female and male TCR^{1640}-transgenic immune cells, independent of the sex of the recipient and of the donor.

Female and male TCR^{1640}-transgenic immune cells have a different gene expression profiles. We hypothesized that female TCR^{1640}-transgenic immune cells and male TCR^{1640}-transgenic immune cells might have distinct RNA expression profiles that drive the difference in disease course, i.e., RR versus progressive disease. We isolated immune cells from their SLOs, differentiated them in vitro, as performed for adoptive transfer, and analyzed these immune cells by transcriptional (RNA) profiling. As a control, we also isolated and differentiated immune cells from SLOs of WT SJL/j male and female mice (Figure 4A). First, we observed that the heat plot between WT male and female immune cells did not reveal major differences. However, when comparing RNA profiles of female and male TCR^{1640}-transgenic immune cells, we found important differences in gene expression patterns (Figure 4B). Different categories of genes were found differently expressed, such as genes involved in immune cell trafficking (*Sell* [L selectin]), immune cell regulation (*Ctla4*), regulation of stress (*Hsp90b1*), neuronal development (*Daglb* [diacylglycerol lipase β]), and posttranslational modifications (*Srpk2* [SRSF protein kinase 2]). We then subtracted the overlap in genes between female TCR^{1640} and female WT SJL/j mice and also subtracted overlapping genes between male TCR^{1640} and male WT SJL/j mice to remove any genes that are inherent to natural sex differences and performed the transcriptome analysis again (see Methods for more information), in this way revealing the genes that are significantly different between the female and male transgenic cells (Figure 4C). Within this data set, we subsequently performed GO enrichment analysis to analyze gene pathways that are upregulated or downregulated in female TCR^{1640}-transgenic immune cells compared with male TCR^{1640}-transgenic immune cells (Figure 4D). In female TCR^{1640}-transgenic immune cells, the negative regulation of T cell immunity was upregulated and contained genes, such as Foxp3, which was then significantly downregulated in male TCR^{1640}-transgenic immune cells (Figure 4E). For more details and information on the analytic approach and raw files, refer to the Supplemental Table 1 and to the Methods.

To conclude, by performing transcriptome analysis, we identified multiple genes that are significantly differently expressed between female and male TCR^{1640}-transgenic immune cells. Interestingly, many genes involved in regulation of T cell–mediated immunity, such as *Ctla4*, *Gpr15*, and *Foxp3*, were upregulated in female TCR^{1640}-transgenic immune cells compared with male transgenic cells.

Discussion

In MS, it is well established that women are more susceptible and develop more often a relapsing form of the disease, while men are overrepresented in the primary progressive course. However, to date no clear explanation for these sex-dependent differences has been identified. To this end, we performed adoptive transfers with transgenic immune cells isolated from male or female TCR^{1640}-transgenic mice,

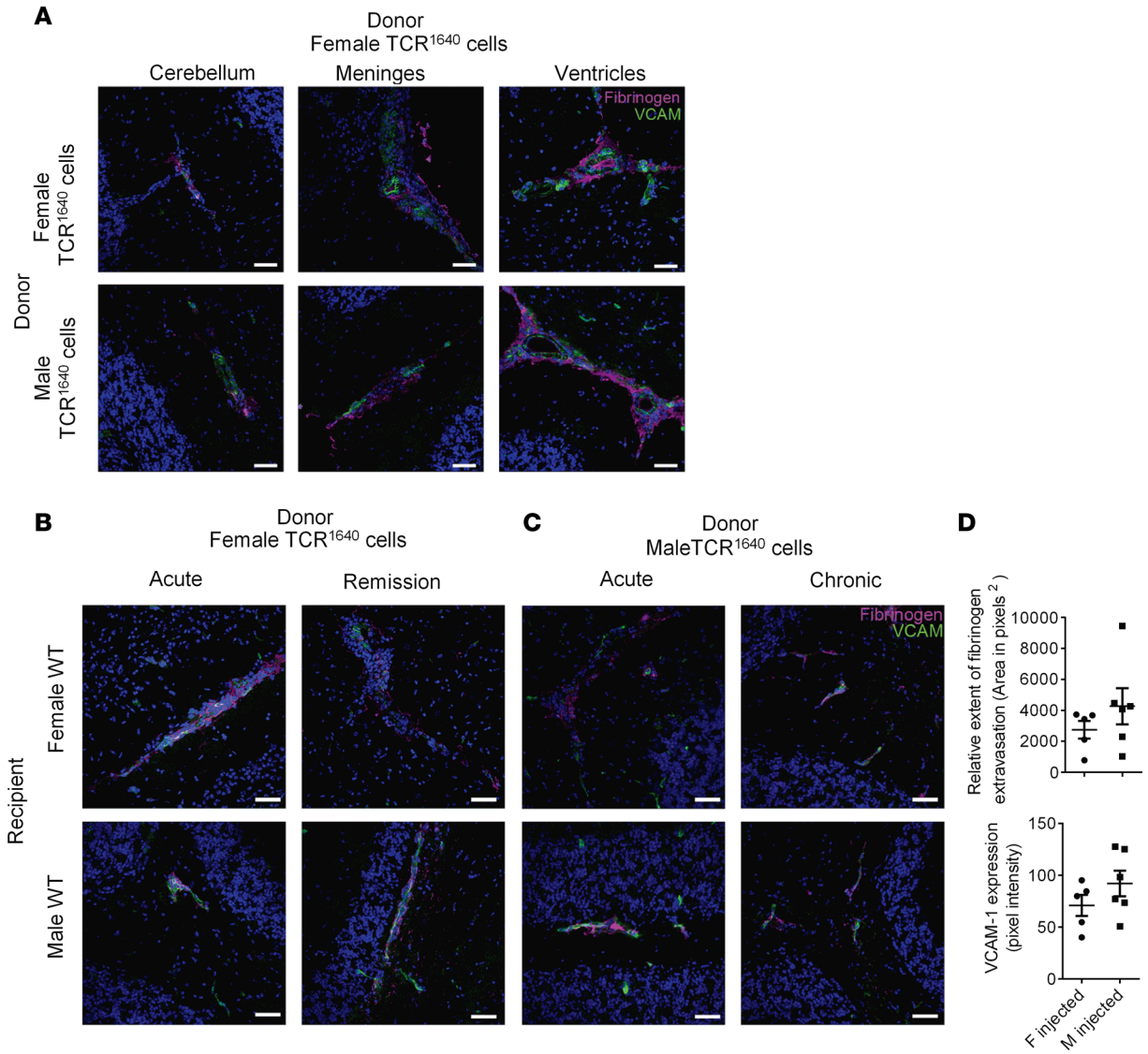

Figure 3. Blood-brain barrier disruption is similar between female and male recipients after adoptive transfer of either male or female TCR^{1640}-transgenic cells. Changes in blood-brain barrier kinetics were analyzed in recipient animals that were sacrificed at first peak of disease (acute, clinical score ≥3) for all transfers, at remission (clinical score of Δ ≥2) for injection of female transgenic cells, and during chronic disease for injection of male transgenic cells (stable clinical score ≥3 for more than 20 days). (**A**) Representative confocal images of fibrinogen extravasation and VCAM-1 expression in cerebellum, meninges, and ventricles of male and female SJL/j recipients after adoptive transfer of female (top) and male (bottom) TCR^{1640} immune cells. (**B**) Representative confocal images of fibrinogen extravasation and VCAM-1 expression in the cerebellum of male and female SJL/j recipients after adoptive transfer of female TCR^{1640} immune cells. (**C**) Representative confocal images of fibrinogen extravasation and VCAM-1 expression in the cerebellum of male and female SJL/j recipients at acute disease after adoptive transfer of male TCR^{1640} immune cells. Images are representative of independent experiments, with at least 3 animals per group. Scale bar: 100 μm. (**D**) Relative levels of expression for VCAM-1 and leakage of fibrinogen were determined by measuring the pixel intensity and area (n = 3–5 per vessel). Data are represented as mean ± SEM, and an unpaired 1-sided t test was used. $P < 0.05$ was considered significant.

who were described to reflect the sex-driven disease course differences seen in MS (5). On the one hand, we observed that transfer of female transgenic cells induced a RR disease, independent of the sex of the recipient. On the other hand, we saw that transfer of male transgenic cells induced a progressive disease, again independent of the sex of the recipient. These data, together with the results of the gene profiling of these cells, demonstrate that underlying sex-dependent factors in the immune compartment can drive different demyelinating disease courses. Of note, female-to-male difference in EAE was reported in certain mouse strains (e.g., SJL/j), while no sex-chromosome effect was detected when using different strains (e.g., C57BL/6) (7). It is therefore important to keep in mind that a model of disease can only shed light on part of the complexity that is seen in the human population.

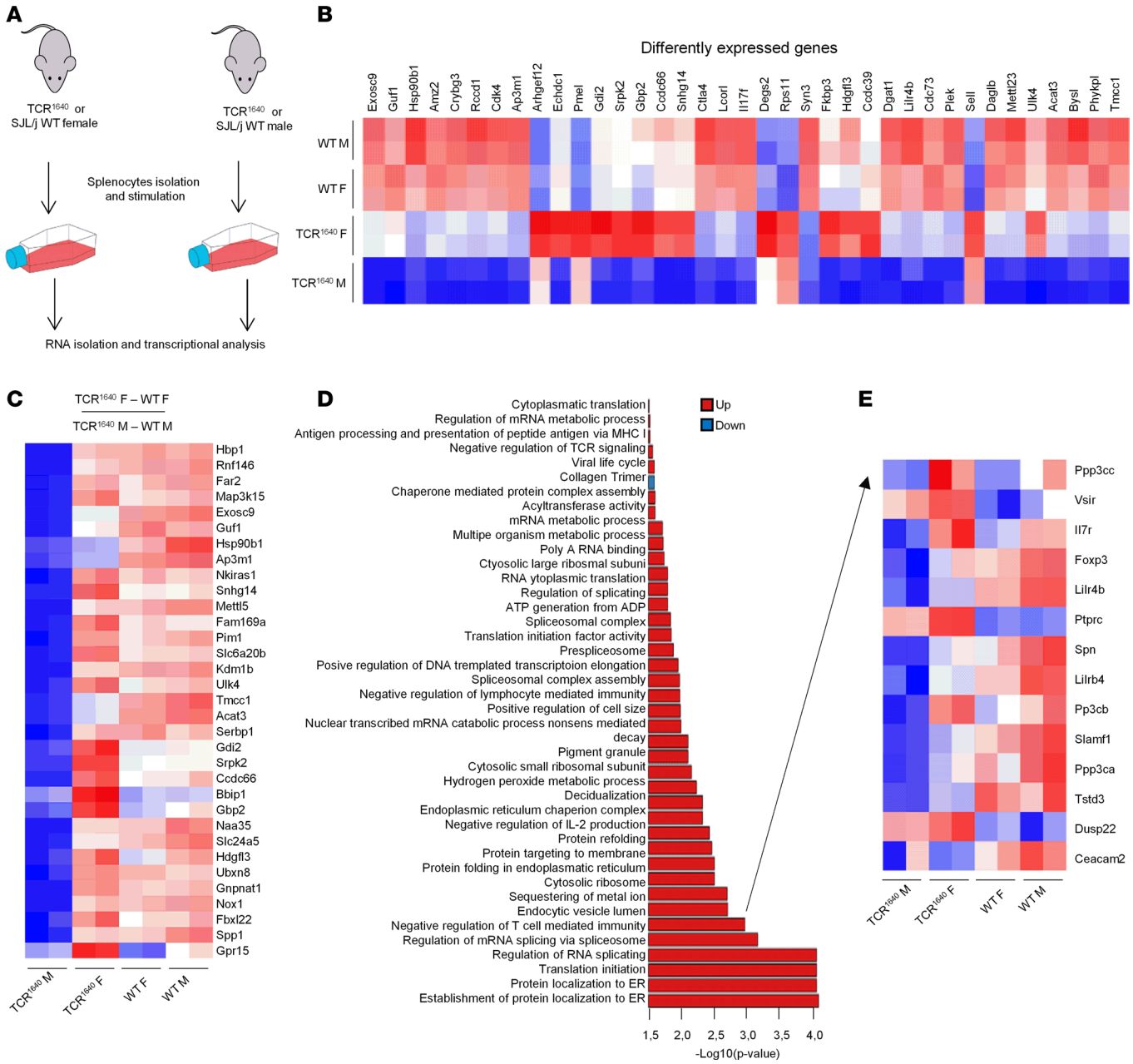

Figure 4. Female and male TCR^{1640}-transgenic immune cells have a different gene expression profile. (**A**) RNA was isolated from immune cells that were Th1/Th17 differentiated and derived from female and male TCR^{1640}-transgenic mice and from male and female SJL/j WT mice for gene expression analysis. (**B**) Differently expressed genes were hierarchically clustered, and the top 65 genes differentially expressed between male TCR^{1640}-transgenic mice, female TCR^{1640}-transgenic mice, male SJL/j WT mice, and female SJL/j WT mice were plotted as a heatmap. Blue indicates low relative expression, and red indicates high relative expression. Rows represent duplicate experiments. (**C**) Differently expressed genes were hierarchically clustered based on the following model: (TCR^{1640} female – SJL/j WT female)/(TCR^{1640} male – SJL/j WT male), and the top 33 genes were plotted as a heatmap. (**D**) GO analysis was performed on the data set described in **C** and shows the analysis of pathways that are significantly upregulated or downregulated in female TCR^{1640}-transgenic mice. (**E**) Differently expressed genes of the pathway negative regulation of T cell–mediated immunity were hierarchically clustered and plotted as a heatmap.

Sex-based differences seen in autoimmune diseases can be inherent to sex hormones or sex chromosomes or a combination of both. Our results show that the sex of the donor cells is responsible for a relapsing or progressive disease, indicating that presence of XX versus the XY, naturally inherent to these immune cells, seems to be important. Notably, however, injection of female cells into female mice or male cells into male mice did result in a more striking disease type (either RR or progressive, respectively), although no significant difference was found between the two recipient groups. Nevertheless, this

shows that, although the immune cells are driving the type of disease, a role for hormones within the recipient animals can still be attributed to influence the severity of the disease. As sex chromosomes are directly linked to sex hormone differences, it would therefore be interesting to further investigate this in an animal model where the sex chromosome compartment is separate from the hormone secretion by the gonads. The 4-core genotype mouse model has a deletion of the Sry gene (the sex-determining region of the Y chromosome) and allows autosomal deletion (XX and XY^-) or insertion (XXSry and XY^-Sry) of the gene, therefore providing the opportunity to compare differences in sex chromosomes while having the same gonadal type (8–11). Given that previous studies using this mouse model have already shown a major role for sex chromosomes in both the immune (7, 8, 12) and neurological compartment (13) during EAE, it would be highly interesting to cross these mice with the TCR^{1640}-transgenic mice and perform adoptive transfers with either XX and XY^- or XXSry and XY^-Sry immune cells. An interesting follow-up would be to use XX versus XY bone marrow chimeras, reconstituted with a common immune system of one sex chromosomal type. This would complement previous reports showing that sex chromosomes can affect neurodegeneration (13).

Th1 and Th17 lymphocytes have been implicated in MS and EAE (14, 15). Some early data suggest that IFN-γ might play a protective role in EAE, as IFN-$\gamma^{-/-}$ mice or mice treated with neutralizing anti–IFN-γ mAb displayed exacerbated disease (16, 17). On the other hand, IL-23–deficient mice, which have later been shown to have smaller numbers of Th17 lymphocytes, did not develop EAE (18–20). Interestingly, we showed that adoptive transfer of male transgenic immune cells, but not of female transgenic cells, leads to a decrease of IL-17 production and an increase in IFN-γ production after acute disease peak. Conversely, increased clustering of $Foxp3^+$ cells was seen in animals at remission after receiving female transgenic cells, while this clustering was not observed in chronically progressing animals that have received male transgenic cells. This is in line with previous studies suggesting that presence of Tregs in EAE leads to a natural recovery after a relapse (21, 22). Overall, these data could indicate a difference between T cell–mediated immune regulation and proliferation of proinflammatory T cells that gives rise to remission or chronic disease after adoptive transfer of either female or male transgenic cells.

Whereas it is well established that in MS different types of disease can be attributed to sex differences, our understanding of how these processes are regulated is just developing. Here, we found that differences in male and female transgenic cells can lead to differences in disease progression, and this is reflected in their gene profile. Among others, numerous genes involved in immune regulation were significantly downregulated in male transgenic cells (*Foxp3*, *Il2ra*, *Ctla4*) or significantly upregulated in female transgenic immune cells (*Gpr15*). GPR15 is a heterotrimeric G protein–coupled receptor that is specialized in controlling the specific homing of $Foxp3^+$ Tregs to the large intestine (23, 24). Of note, GPR15 expression differs in the effector and Treg subsets of humans versus those of mice (25, 26). These regulatory genes could provide possible targets to explore the difference seen in female induced remitting disease compared with progressive disease without recovery. In addition, when comparing female with male transgenic immune cells, various pathway involved in negative regulation of T cell–mediated immunity were upregulated in female transgenic cells. These results are in line with a comparative analysis of leukocytes isolated from RRMS patients in remission or during relapse, where a sex-specific coexpression of genes was found (27).

To conclude, further unraveling the underlying mechanisms that are responsible for sex-dependent differences seen in MS opens up avenues toward more personalized medicine and novel targets that can be used as natural disease modifiers (4).

Methods

Adoptive transfer EAE with TCR^{1640}-transgenic mice. Female and male TCR^{1640}-transgenic mice were obtained through a collaboration with the lab of Hartmut Wekerle in Germany. Spleens and lymph nodes from presymptomatic mice (mice at 35 to 55 days old) were harvested, and immune cells were isolated as previously described (28). Cells were cultured for 4 days as previously described (29). Briefly, cells were stimulated in RPMI supplemented with 10% fetal bovine serum, nonessential amino acids, HEPES, and β-mercaptoethanol in the presence of recombinant mouse IL-23 (20 ng/ml), recombinant human TGF-β (4 ng/ml), recombinant mouse IL6 (20 ng/ml), recombinant mouse IL-12 (3 ng/ml), and mouse anti-CD3 (1 μg/ml). A total cell suspension of 20–25 million immune cells was then injected into the tail veins of age-matched female and male WT SJL/j littermates. Recipient mice were injected intraperitoneally with

a single pertussis toxin dose (200 ng) 2 days after the adoptive transfer. As a control, immune cells isolated from spleens and lymph nodes of WT SJL/j females and males were also injected i.v. after stimulation into age-matched female and male WT SJL/j mice. These control mice also received a single pertussis toxin dose (200 ng) 2 days after the transfer. Mice were weighed and scored daily based on the functional effect of paralysis and/or ataxia as follows: 1.0 = no control tail or mild balance impairment with mild head turn or both (1.5); 2 = righting reflex impaired either due to paralysis or ataxia or both (2.5); 3 = reaching a score of 3 on either atypical or typical EAE scoring scale or both (3.5); 4 = reaching a score of 4 on either atypical or typical EAE scoring scale or both (4.5); 5 = moribund.

Harvest of tissue at acute, remission, and chronic phase. After induction of disease by adoptive transfer, animals were sacrificed at different time points for further analysis. Mice that received male TCR^{1640} or WT cells were sacrificed at first peak (acute, clinical score ≥3, day 6 ± 0.5 after injection) of the disease and at chronic phase (same clinical score of at least 3 for ≥20 days), while mice who received female TCR^{1640} or WT cells were sacrificed at first peak (acute, clinical score ≥3, day 6 ± 0.5 after injection) of the disease and at remission (Δ of scores of at least 2, between first maximum score at relapse and the first minimum score at remission, day 14.7 ± 1.7). Brains, spinal cords, spleens, and lymph nodes were harvested and frozen for immunostaining and/or immune cells were isolated for flow cytometry as previously described (28).

Flow cytometry. Immune cells were analyzed with flow cytometry prior to injection to their profile. Immune cells isolated from brains, spinal cords, spleens, and lymph nodes at peak, remission, or chronic disease were stained as previously described (28). A Live/Dead staining (Thermo Fisher) was added for all stainings. For surface staining, CD4 PE-Cy7 (552775, clone RM4-5), CD8 Pacific Blue (558106, clone 53-6.7), CD45 Percp-cy5.5 (550994, clone 30-F11), Vα8.3 FITC (553376, clone B21.14), and Vβ4 BV711 (743023, clone KT4) (all from BD Biosciences) and CD11b BV785 (101243, clone M1/70, Biolegend) were used. For intracellular staining, cells were labeled with IL-17 BV605 (564169, clone TC11-18H10) and IFN-γ APC (554413, clone XMG1.2) (all from BD Biosciences). The appropriate isotypes were used from intracellular cytokine staining. Cells were acquired on a BD LSR II and analyzed using BD FACS-Diva software and FlowJo software.

Luxol fast blue and H&E staining. Brains and spinal cords from mice at peak, remission, and chronic disease were cut into 7-μM sections and stained with Luxol fast blue and H&E as previously described (30). Images were made using a Leica DM6000 microscope with Improvision OpenLab 4.0.4 software.

Immunofluorescent stainings. Brains and spinal cords from mice at peak, remission, and chronic disease were cut into 7-μM sections and used for immunofluorescent stainings. To stain CD4 and Foxp3, slides were air dried for 30 minutes and dipped in cold acetone for 5 minutes to air dry them again for 30 minutes. After several washing steps, the sections were blocked with 10% donkey serum and treated with the endogenous biotin-blocking kit (Thermo Fisher, E21390). The primary antibody against CD4 (anti-rat CD4, BD558107) was added for 1 hour. After several washing steps, the secondary antibody (donkey anti-rat; Invitrogen, A21208) was added. After several washing steps and blocking with rat serum, the primary antibody against Foxp3 (anti-mouse Foxp3; ebioscience, 13-5773-82) was added for 1 hour. After several washing steps, the secondary antibody (Streptavidin Jackson, 016-160-084) was added for 1 hour. Finally, the slides were mounted in Mowiol (MilliporeSigma) containing TOPRO-3 (1:300; Invitrogen). Immunofluorescent stainings for VCAM and fibrinogen were done as previously described (30). Images were acquired with a Leica SP5 confocal microscope and analyzed with the Leica LAS AF software.

Quantification and statistical analysis of confocal images. Images (*Z*-stacks) were acquired using a Leica SP5 confocal microscope with Leica LAS AF software and processed using Fiji and LAS X. All settings were kept the same. Disruption of the BBB (VCAM-1 expression) and differences in fibrinogen leakage were quantified by measuring the mean intensity of positive pixels (0 [black, lowest intensity] to 255 [white, highest intensity]) and the total area of extravasation. The number of $Foxp3^+$ and $CD4^+$ cells were counted to calculate the percentage of $Foxp3^+$ cells within each staining. Data were analyzed blinded, and an unpaired *t* test was used to test for statistical differences.

RNA isolation, library preparation, and whole-genome RNA sequencing. Total immune cells that were isolated from spleens and lymph nodes of TCR^{1640} or WT SJL/j mice were differentiated as described above. A total of 5 million cells was taken and resuspended in Trizol (Life Technologies, 15596018) and frozen at –80°C until needed. RNA was isolated using the standard RNeasy mini kit (Qiagen,

74104) according to the manufacturer's guidelines. Samples were stored at –80°C until needed for whole-genome RNA sequencing.

A total of 500 ng RNA was used for library preparation. Quality of total RNA was assessed with the BioAnalyzer Nano (Agilent), and all samples had a RIN above 9.2. Library preparation was done with the KAPA mRNAseq stranded kit (KAPA, KK8420). Ligation was made with 10 nM final concentration of Illumina index, and 9 PCR cycles were required to amplify cDNA libraries. Libraries were quantified by QuBit and BioAnalyzer DNA1000. All libraries were diluted to 10 nM and normalized by qPCR using the KAPA library quantification kit (KAPA, KK4973). Libraries were pooled to equimolar concentrations. Sequencing was performed with the Illumina Nextseq500 using 1.5 Nextseq High Output Kit (75 cycles) run with 2 pM of the pooled library. Around 200 M single-end PF reads were generated per sample. Library preparation and sequencing were done at the Institute for Research in Immunology and Cancer's Genomics Platform.

Analysis of whole-genome RNA sequencing. Quality control was performed using FastQC (http://www.bioinformatics.babraham.ac.uk/projects/fastqc), a quality control tool for high-throughput sequence data. Next, alignment to the reference genes (Genome Reference Consortium Mouse Build 38, *Mus musculus*, mm10) was done using Bowtie2 (31). The model for subtraction was as follows: female difference = TCR^{1640}_female – SJL/j WT _female and male difference = TCR^{1640}_male – SJL/j WT _male, so the overall difference = (TCR^{1640}_female – SJL/j WT _female) – (TCR^{1640}_male SJL/j WT _male). The top 33 genes that were significantly upregulated or downregulated ($P < 0.05$) are shown. Quantification of the gene expression level was performed using HTSeq (32). A quality control check was performed on the count matrix with principal component analysis to ensure the absence of batch effect. To analyze differentially expressed genes, a combination of Limma and EdgeR libraries was used (33, 34). Finally, graphical representation into volcano plots and heat map was performed using R software (R Core Team, 2016). The analysis was performed at the CRCHUM Bioinformatics platform. The model that was used for differential expression of TCR^{1640} cells versus SJL/j WT cells is as follows: fold change of expression of TCR^{1640} mice/expression of SJL/j mice. The exponentially distributed data were then logarithmically transformed into $\log_2$(expression) with logb (x/y) = logb (x) – logb (y). The model for subtraction was as follows: female difference = TCR^{1640}_female – SJL/j WT _female and male difference = TCR^{1640}_male – SJL/j WT _male, so the overall difference = (TCR^{1640}_female – SJL/j WT _female) – (TCR^{1640}_male- SJL/j WT _male). The RNA-sequencing data have been deposited in a MINSEQE-compliant public database (GEO accession GSE125913).

Statistics. Data are presented as mean ± SEM unless otherwise indicated. Sample number (n) indicates the number of independent biological samples in each experiment. Data are considered to be statistically significant when $P < 0.05$ by unpaired 2-tailed Student's t test, paired Student's t test, or 1-way ANOVA, as indicated in the figure legends. In the figures, asterisks denote statistical significance. Statistical analysis was performed with the Graphpad Prism 6.0 software.

Study approval. All experiments were approved by the University of Montreal Animal Care committee (N11023APs) and followed the guidelines of the Canadian Council on Animal Care.

Author contributions

TD and AP designed the research studies and wrote the paper. TD, CL, and LT optimized and conducted the experiments. TD acquired and analyzed the data. CG, LB, SL, OSL, MAL, RMR, and SZ helped conduct experiments.

Acknowledgments

This work was funded by an operating grant from the Canadian Institutes of Health Research (MOP 89885, PJI-153195). TD holds a postdoctoral fellowship from the Fonds de la Recherche en Santé du Québec. AP holds the T1 (senior) Canada Research Chair in MS. We thank Hartmut Wekerle for providing us with the TCR^{1640} mice. We would also like to thank the bioinformatics platform, the imaging platform, and the flow cytometry platform from CRCHUM for the excellent technical guidance and support and Alice M. Roy and Elvia Gonzalez for their excellent technical animal support.

Address correspondence to: Alexandre Prat, CRCHUM, 900 rue Saint Denis, Tour Viger, H2X-0A9, Montréal, Québec, Canada. Phone: 1.514.890.8000; Email: a.prat@umontreal.ca.

1. Trojano M, et al. Geographical variations in sex ratio trends over time in multiple sclerosis. *PLoS ONE*. 2012;7(10):e48078.
2. Bove R, Chitnis T. The role of gender and sex hormones in determining the onset and outcome of multiple sclerosis. *Mult Scler*. 2014;20(5):520–526.
3. Ortona E, Pierdominici M, Maselli A, Veroni C, Aloisi F, Shoenfeld Y. Sex-based differences in autoimmune diseases. *Ann Ist Super Sanita*. 2016;52(2):205–212.
4. Golden LC, Voskuhl R. The importance of studying sex differences in disease: The example of multiple sclerosis. *J Neurosci Res*. 2017;95(1-2):633–643.
5. Pöllinger B, et al. Spontaneous relapsing-remitting EAE in the SJL/J mouse: MOG-reactive transgenic T cells recruit endogenous MOG-specific B cells. *J Exp Med*. 2009;206(6):1303–1316.
6. Absinta M, Sati P, Reich DS. Advanced MRI and staging of multiple sclerosis lesions. *Nat Rev Neurol*. 2016;12(6):358–368.
7. Voskuhl RR, Pitchekian-Halabi H, MacKenzie-Graham A, McFarland HF, Raine CS. Gender differences in autoimmune demyelination in the mouse: implications for multiple sclerosis. *Ann Neurol*. 1996;39(6):724–733.
8. Smith-Bouvier DL, et al. A role for sex chromosome complement in the female bias in autoimmune disease. *J Exp Med*. 2008;205(5):1099–1108.
9. Arnold AP, Chen X. What does the "four core genotypes" mouse model tell us about sex differences in the brain and other tissues? *Front Neuroendocrinol*. 2009;30(1):1–9.
10. Lovell-Badge R, Robertson E. XY female mice resulting from a heritable mutation in the primary testis-determining gene, Tdy. *Development*. 1990;109(3):635–646.
11. Mahadevaiah SK, et al. Mouse homologues of the human AZF candidate gene RBM are expressed in spermatogonia and spermatids, and map to a Y chromosome deletion interval associated with a high incidence of sperm abnormalities. *Hum Mol Genet*. 1998;7(4):715–727.
12. Voskuhl RR. Chronic relapsing experimental allergic encephalomyelitis in the sjl mouse: relevant techniques. *Methods*. 1996;10(3):435–439.
13. Du S, Itoh N, Askarinam S, Hill H, Arnold AP, Voskuhl RR. XY sex chromosome complement, compared with XX, in the CNS confers greater neurodegeneration during experimental autoimmune encephalomyelitis. *Proc Natl Acad Sci USA*. 2014;111(7):2806–2811.
14. Zamvil SS, Steinman L. The T lymphocyte in experimental allergic encephalomyelitis. *Annu Rev Immunol*. 1990;8:579–621.
15. Kebir H, et al. Preferential recruitment of interferon-gamma-expressing TH17 cells in multiple sclerosis. *Ann Neurol*. 2009;66(3):390–402.
16. Ferber IA, et al. Mice with a disrupted IFN-gamma gene are susceptible to the induction of experimental autoimmune encephalomyelitis (EAE). *J Immunol*. 1996;156(1):5–7.
17. Chu CQ, Wittmer S, Dalton DK. Failure to suppress the expansion of the activated CD4 T cell population in interferon gamma-deficient mice leads to exacerbation of experimental autoimmune encephalomyelitis. *J Exp Med*. 2000;192(1):123–128.
18. Cua DJ, et al. Interleukin-23 rather than interleukin-12 is the critical cytokine for autoimmune inflammation of the brain. *Nature*. 2003;421(6924):744–748.
19. Ghoreschi K, et al. Generation of pathogenic T(H)17 cells in the absence of TGF-β signalling. *Nature*. 2010;467(7318):967–971.
20. Gaffen SL, Jain R, Garg AV, Cua DJ. The IL-23-IL-17 immune axis: from mechanisms to therapeutic testing. *Nat Rev Immunol*. 2014;14(9):585–600.
21. McGeachy MJ, Stephens LA, Anderton SM. Natural recovery and protection from autoimmune encephalomyelitis: contribution of CD4+CD25+ regulatory cells within the central nervous system. *J Immunol*. 2005;175(5):3025–3032.
22. Stephens LA, Gray D, Anderton SM. CD4+CD25+ regulatory T cells limit the risk of autoimmune disease arising from T cell receptor crossreactivity. *Proc Natl Acad Sci USA*. 2005;102(48):17418–17423.
23. Kim SV, et al. GPR15-mediated homing controls immune homeostasis in the large intestine mucosa. *Science*. 2013;340(6139):1456–1459.
24. Konkel JE, et al. Transforming growth factor-β signaling in regulatory T cells controls T helper-17 cells and tissue-specific immune responses. *Immunity*. 2017;46(4):660–674.
25. Bilsborough J, Viney JL. GPR15: a tale of two species. *Nat Immunol*. 2015;16(2):137–139.
26. Nguyen LP, et al. Role and species-specific expression of colon T cell homing receptor GPR15 in colitis. *Nat Immunol*. 2015;16(2):207–213.
27. Irizar H, et al. Transcriptomic profile reveals gender-specific molecular mechanisms driving multiple sclerosis progression. *PLoS ONE*. 2014;9(2):e90482.
28. Kebir H, et al. Human TH17 lymphocytes promote blood-brain barrier disruption and central nervous system inflammation. *Nat Med*. 2007;13(10):1173–1175.
29. Larochelle C, et al. Melanoma cell adhesion molecule identifies encephalitogenic T lymphocytes and promotes their recruitment to the central nervous system. *Brain*. 2012;135(Pt 10):2906–2924.
30. Alvarez JI, et al. Focal disturbances in the blood-brain barrier are associated with formation of neuroinflammatory lesions. *Neurobiol Dis*. 2015;74:14–24.
31. Langmead B, Salzberg SL. Fast gapped-read alignment with Bowtie 2. *Nat Methods*. 2012;9(4):357–359.
32. Anders S, Pyl PT, Huber W. HTSeq--a Python framework to work with high-throughput sequencing data. *Bioinformatics*. 2015;31(2):166–169.
33. Ritchie ME, et al. limma powers differential expression analyses for RNA-sequencing and microarray studies. *Nucleic Acids Res*. 2015;43(7):e47.
34. Robinson MD, McCarthy DJ, Smyth GK. edgeR: a Bioconductor package for differential expression analysis of digital gene expression data. *Bioinformatics*. 2010;26(1):139–140.